Current Biology, Vol. 13, 1480–1487, September 2, 2003, ©2003 Elsevier Science Ltd. All rights reserved. DOI 10.1016/S0960-9822(03)00580-3

PIR121 Regulates Pseudopod Dynamics and SCAR Activity in *Dictyostelium*

Simone L. Blagg, Michael Stewart, Christine Sambles, and Robert H. Insall*
School of Biosciences
University of Birmingham
Edgbaston
Birmingham B15 2TT
United Kingdom

Summary

Background: The WASP/SCAR family of adaptor proteins coordinates actin reorganization by coupling different signaling molecules, including Rho-family GTPases, to the activation of the Arp2/3 complex. WASP binds directly to Cdc42 through its GTPase binding domain (GBD), but SCAR does not contain a GBD, and no direct binding has been found. However, SCAR has recently been found to copurify with four other proteins in a complex. One of these, PIR121, binds directly to Rac.

Results: We have identified four of the members of this complex in *Dictyostelium* and disrupted the *pir*A gene, which encodes PIR121. The resulting mutant cells are unusually large, maintain an excessive proportion of their actin in a polymerized state and display severe defects in movement and chemotaxis. They also continually extend new pseudopods by widening and splitting existing leading edges rather than by initiating new pseudopods. Comparing these cells to *scar* null mutants shows behavior that is broadly consistent with overactivation of SCAR. Deletion of the *pir*A gene in a *scar*$^-$ mutant resulted in cells resembling their *scar*$^-$ parents with no obvious changes, confirming that PIR121 mainly acts through SCAR in vivo. Surprisingly given their hyperactive phenotype, we find that *pir*A$^-$ mutants contain very little intact SCAR protein despite normal levels of mRNA, suggesting a posttranscriptional downregulation of activated SCAR.

Conclusions: Our results demonstrate a genetic connection between the *pir*A and *scar* genes. PIR121 appears to inhibit the activity of SCAR in the absence of activating signals. The location of the newly formed protrusions indicates that unregulated SCAR is acting at the edges of existing pseudopods, not elsewhere in the cell. We suggest that active SCAR protein released from the inhibitory complex is rapidly removed and that this is an important and novel mechanism for controlling actin dynamics.

Introduction

Actin polymerization is the driving force for numerous cell processes involving movement and shape change. Cell motility requires cycles of actin polymerization and depolymerization, and this is tightly regulated by Rho-family GTPases, which relay signals to the actin polymerization machinery of the cell, most notably to the Arp2/3 complex. This seven-membered complex can nucleate de novo actin polymerization by using existing filaments as templates, and it thus produces a network of branched actin filaments at the leading edge [1, 2]. However, the Arp2/3 complex alone is not sufficient for actin filament production in vivo; additional proteins that bind and activate the complex are required. Members of the WASP/SCAR family of adaptor proteins are the best understood Arp2/3 activators and are thought to interact through a conserved acidic domain at their C termini [3] and thus to induce a conformational change that enables the complex to nucleate actin [4].

The mammalian WASP/SCAR family currently consists of five members, WASP (Wiskott-Aldrich Syndrome protein) [5], N-WASP (the more widely expressed relative of WASP) [6], and three SCAR isoforms (SCAR 1–3) [7], which are also known as WAVEs (WASP/verprolin homologous proteins) [8]. SCAR was initially discovered in the amoeba *Dictyostelium discoideum*, as a second-site suppressor of a deletion in the gene encoding cAMP receptor cAR2 [9]. It was subsequently identified as a WASP-related protein that was capable of activating the Arp2/3 complex [3, 10]. Disruption of the SCAR gene in *Dictyostelium* gives rise to small cells with reduced F-actin levels and movement defects [9]. Recently, in vivo studies in *Drosophila* have shown that its SCAR localizes to actin-rich structures and is required for normal cell morphology throughout development (as is the Arp2/3 complex), whereas WASP is largely dispensable [11].

WASP/SCAR proteins are thought to couple Rho-family GTPases to the cytoskeleton. WASP interacts with Cdc42 through its GTPase binding domain (GBD) [6, 12]. It is regulated in part by autoinhibition; isolated, native WASP has been found to be inactive until stimulated [13]. The N-terminal domain, (including the GBD domain) normally binds to the C-terminal domain (which is responsible for binding to the Arp2/3 complex), and this autoinhibition can be relieved when Cdc42 interacts with the GBD domain and causes a conformational change in the protein [13, 14].

The mechanism of SCAR regulation has proved harder to expose, mainly because of the lack of signal-related domains in the sequence of SCAR proteins. It is generally thought that SCAR is somehow coupled to Rac, which is involved in the pathway leading to production of lamellipodia [8], where SCAR is recruited in mammalian cells [15]. However, direct binding to Rac has not been found [8]. In addition, pure SCAR protein is constitutively active [10]. Recent work has identified a complex of proteins that are bound to SCAR to form an inactive complex [16]. These candidate proteins have been identified as Nap125, PIR121, Abi2, and HSPC300.

Nap125 (Nck-associated protein) was first identified in a screen for Nck binding proteins [17], and its expression is downregulated in Alzheimer's disease [18, 19]. Nap125 was found to interact with Rac indirectly through a 140 kd protein [20], which is now known as PIR121

*Correspondence: r.h.insall@bham.ac.uk

(p53-inducible mRNA) [21]. A mammalian homolog of PIR121 named p140Sra-1 (p140 Specifically Rac-associated protein-1), is known to interact specifically and directly with GTP-charged Rac1 through its N-terminal domain [22]. Abl interactor 2 (Abi2) is an SH3 domain-containing protein that has been implicated in cytoskeletal function and cell migration [23] and is located at sites of actin polymerization [24].

The complex containing inactive SCAR may be disassembled by the binding of activated Rac and Nck, presumably to PIR121 and Nap125, releasing active SCAR that is then free to contact the Arp2/3 complex [16]. This in-vitro work has yet to be proven in vivo, although a recent, unrelated study in *C. elegans* has implicated both PIR121 and Nap125 (termed GEX-2 and GEX-3, respectively) in regulation of cell migration and shape change [25].

In this work we identify the proposed members of the SCAR inhibitory complex in *Dictyostelium* and find them to be well conserved. We show that mutants in the gene that encodes PIR121 (termed *pir*A in *Dictyostelium*) are affected in multiple aspects of cell motility in a way that is consistent with unregulated SCAR activity. We also find that SCAR protein levels are apparently regulated by their interaction with PIR121.

Results

Identification of Genes Encoding PIR121 and Other SCAR Complex Members in *Dictyostelium*

Dictyostelium SCAR is highly homologous to the SCAR/WAVE proteins of mammals. We therefore searched for *Dictyostelium* homologs of the four other members of the proposed SCAR regulatory complex [16]. We found single genes encoding PIR121, Nap125, HSPC300, and Abi2 represented in both the Tsukuba *Dictyostelium* cDNA project and the *Dictyostelium* genome project. All four predicted proteins are highly homologous to their mammalian counterparts, being 35%, 23%, 25%, and 18% identical, respectively, throughout their lengths (shown in Figures S1–S4 in the Supplemental Data available with this article online). We then generated a *pir*A null *Dictyostelium* mutant. The *pir*A$^-$ cells have no obvious developmental defects and form normal fruiting bodies when starved on non-nutrient agar plates (data not shown).

To confirm that the phenotype of the *pir*A null cells was not generated or altered during selection for loss of *pir*A, we generated independent mutant strains by transfecting DIR-1 diploid cells (Jason King and R.H.I., in press, BMC Cell Biology) to make heterozygous disruptants that we could then use to segregate fresh *pir*A$^-$ haploids.

Several of the phenotypes described below suggested that deletion of the *pir*A gene caused an inappropriate activation of the SCAR protein. We therefore constructed a *scar*$^-$ and *pir*A$^-$ double mutant.

*pir*A Mutant Cells are Large and Migrate Poorly

Disruption of the *pir*A gene yielded cells with an unusual, severe, highly motile phenotype. Figure 1 shows DIC images of a typical wild-type (AX3), a *pir*A$^-$ mutant, a *scar*$^-$ mutant, and a double *pir*A$^-$/*scar*$^-$ mutant cell. It is immediately apparent that *pir*A$^-$ cells are abnormally large, with extensive hyaline protrusions, whereas in comparison *scar* null cells are slightly smaller than wild-type cells and have fewer protrusions, in accordance with previous data on the *scar* null phenotype [9]. It seemed possible that the mutant cells were larger because of a defect in cytokinesis. However, Hoechst 33342 staining showed no obvious difference between the numbers of nuclei in wild-type and *pir*A$^-$ cells (data not shown). Conversely, double *pir*A$^-$/*scar*$^-$ mutants show none of the phenotypes exhibited by *pir*A$^-$ mutants and instead appear to have a simple *scar* null phenotype.

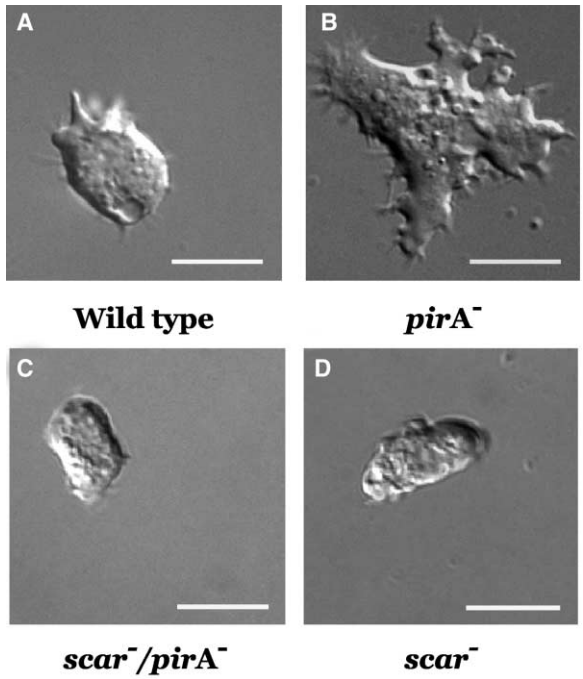

Figure 1. *pir*A$^-$ Cells Are Large with Abnormal Morphology

Bacterially grown wild-type (AX3), *pir*A null, *pir*A$^-$/*scar*$^-$, and *scar* null cells were allowed to adhere to a glass coverslip and are observed with Nomarski differential interference contrast. The scale bars represent 10 μm.

We examined the movement of *pir*A$^-$ cells by using time-lapse microscopy (Movie 2 in the Supplemental Data). Their motility is highly abnormal, and they are also more spread out than normal and appear to have defects in adhesion. The large protrusions seen in mutant cells (Figure 1) are constantly being extended and retracted, indicating that the large hyaline areas are caused by an excessive rate of initiation of new pseudopods rather than by generation of excessively large pseudopods per se. It is also clear that *pir*A$^-$ cells have difficulties in retracting existing protrusions. Long extensions are frequently seen, and these are revealed in time-lapse movies to be very long retraction fibers (Movie 2). Similar problems have been seen in other signal transduction mutants, in particular *ras*G$^-$ and *pak*A$^-$ cells [26, 27].

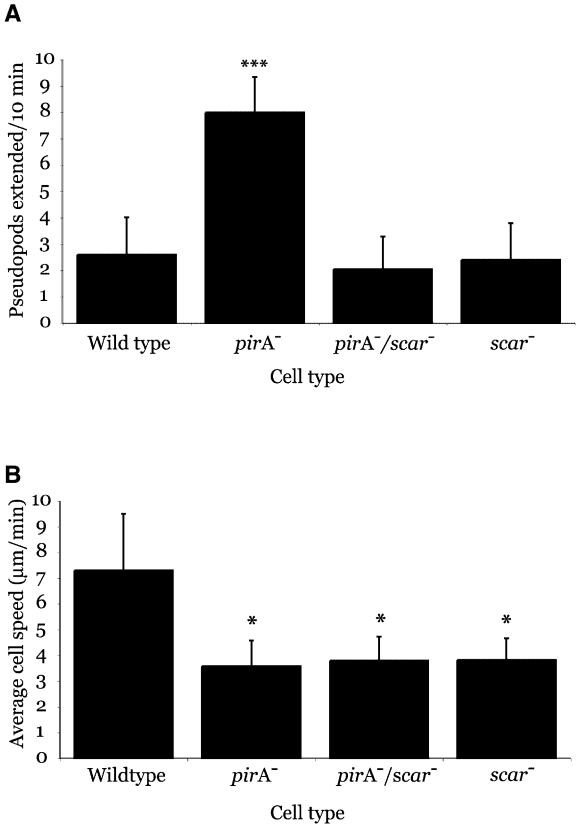

Figure 2. Movement of *pir*A$^-$, *scar*$^-$, and *pir*A$^-$/*scar*$^-$ Mutant Cells

(A) *pir*A$^-$ cells extend an abnormally large number of pseudopods. Wild-type (AX3), *pir*A null, *pir*A$^-$/*scar*$^-$, and *scar* null cells were filmed under Nomarski differential interference contrast, and the number of pseudopods extended over a period of 10 min was scored. Values represent averages of 20 cells, and error bars show one standard deviation. The number of pseudopods in *pir*A$^-$ cells was found to be significantly higher than in wild-type *scar*$^-$ and *pir*A$^-$/*scar*$^-$ cells ($P < 0.01$).

(B) Impaired movement of *pir*A$^-$, *pir*A$^-$/*scar*$^-$, and *scar*$^-$ cells. The average speed of wild-type (AX3), *pir*A$^-$, *pir*A$^-$/*scar*$^-$, and *scar*$^-$ cells was calculated after analysis of time-lapse DIC movies. Error bars represent one standard deviation. *pir*A$^-$, *scar*$^-$, and *pir*A$^-$/*scar*$^-$ cells were found to be significantly slower than wild-type ($P < 0.01$).

We counted the number of hyaline pseudopods extended by cells in time-lapse videos. As shown in Figure 2A, *pir*A$^-$ cells extend pseudopods at more than three times the rate of wild-type cells. *scar* null and *pir*A$^-$/*scar*$^-$ cells extend far fewer pseudopods than *pir*A$^-$ cells but are still capable of generating the usual range of actin structures (Figure 2A and Movie 3). This contradicts previous suggestions that SCAR is required for specific classes of actin structure [28].

The highly active motility of *pir*A null cells leads, paradoxically, to a serious slowing of overall cell movement (Figure 2B). We presume that the lack of control of protrusion and actin polymerization is responsible for the slow cell speed because generation of new pseudopods around the cell periphery decreases directionality and efficiency of movement. The *scar*$^-$ and *pir*A$^-$/*scar*$^-$ mutants also display slow movement (Figure 2B), but in contrast, this appears to be due to decreased actin polymerization and a reduction in the number of cell protrusions.

Excessive Actin Polymerization in *pir*A$^-$ Mutants

Determination of filamentous actin content by isolation of the Triton-insoluble cytoskeleton provides a striking demonstration of the phenotype of *pir*A$^-$ cells. Resting *pir*A null cells contain a very high proportion of F-actin relative to total cellular actin (Figure 3A). This is consistent with the large number of actin-rich protrusions in the mutant cells, even in the absence of chemotactic stimuli (Figures 1 and 2A and Movie 2). This proportion of polymerized actin is as high as has been seen in any mutant. It is comparable with that seen in profilin double nulls [29], which are almost immobile, and greater than that seen in racGAP nulls [30]. This high proportion of F-actin is not found in the double *pir*A$^-$/*scar*$^-$ mutant, which instead has an F-actin content comparable to that of its *scar*$^-$ parent and wild-type cells.

We also used a phalloidin binding assay [31] to measure changes in F-actin content in response to a chemotactic stimulus (Figure 3B). Somewhat unexpectedly, we found that the F-actin content rises rapidly after addition of cAMP to *pir*A, *scar*, and double *pir*A/*scar* mutants, showing that SCAR and its regulatory complex are not required for chemoattractant-induced actin polymerization. Again, *pir*A null cells have an abnormally high F-actin content both before and after stimulation under these assay conditions (Figure 3B). Figure 3C shows F-actin staining of wild-type and *pir*A mutants; *pir*A null cells are bigger than wild-type, whereas *pir*A$^-$/*scar*$^-$ double mutants resemble *scar*$^-$ mutants, which are small with fewer actin structures.

Chemotaxis of *pir*A$^-$ and *scar*$^-$ Mutants

Dictyostelium cells can force themselves under a thin layer of agarose in order to move up a gradient of folate [32], which allows a versatile assay for chemotaxis. We performed under-agar assays on *pir*A$^-$, *scar*$^-$, and *pir*A$^-$/*scar*$^-$ cells. As we had observed in the actin polymerization assay, all three cell lines are able to detect and move up chemotactic gradients, albeit less efficiently than wild-type cells (Supplemental Data, Movies 5–8). For all mutants, chemotaxis was impaired in both accuracy of direction (measured by the chemotactic index) and speed of movement toward the stimulus (Figure 4). In addition, the fronts of *pir*A$^-$ cells were found to continuously generate new pseudopods while moving under agar, whereas *scar*$^-$ and *pir*A$^-$/*scar*$^-$ cells initiate fewer protrusions than wild-type during chemotaxis (Figure 4 and Movies 5–12). It is likely that this property of *pir*A null cells, as well as the other movement defects described earlier, are the reasons for decreased efficiency of chemotaxis because the connections between signaling and actin polymerization seem to be relatively intact (see Figure 3B). In other words, the defects in *pir*A null cells are caused by a decreased ability to orient and in general to move effectively rather than by impaired perception or transduction of chemotactic stimuli.

Formation of New Protrusions by the Splitting of Existing Pseudopods

As can be clearly seen in Movie 2, most of the new pseudopods that are made in *pir*A$^-$ cells originate from

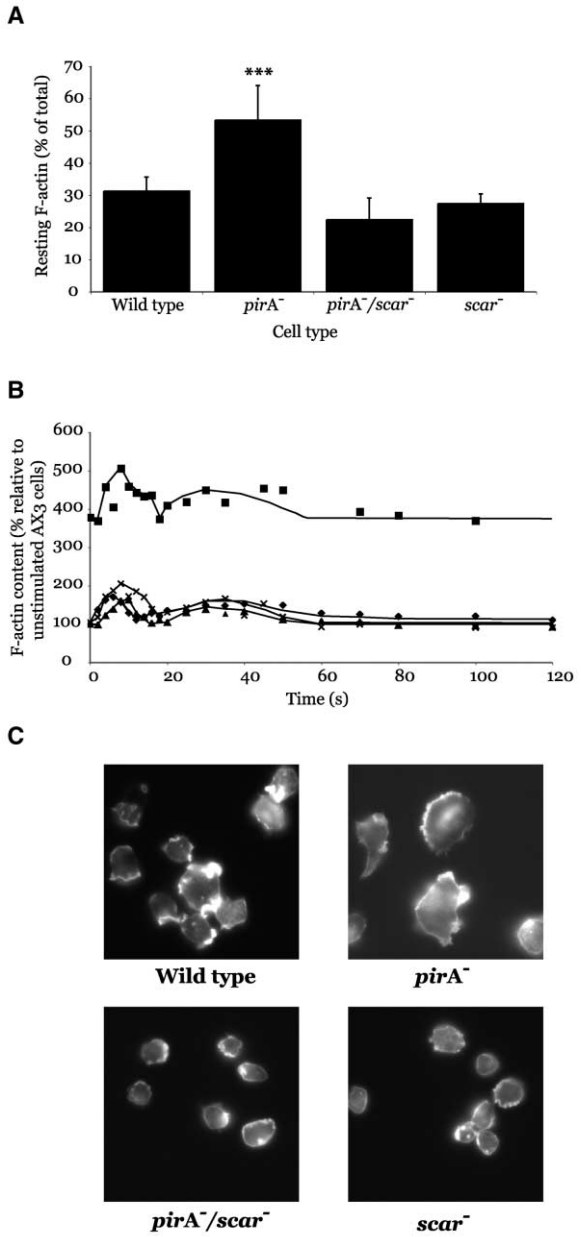

Figure 3. Actin Dynamics in *pir*A$^-$, *scar*$^-$, and *pirA*$^-$/*scar*$^-$ Mutant Cells

(A) High proportion of polymerized actin in *pir*A$^-$ cells. The quantities of actin in the Triton-insoluble cytoskeleton and whole cells were determined by Coomassie staining of PAGE gels. Resting *pir*A$^-$ cells contain a significantly larger percentage of their actin in a polymerized state than resting wild-type, *scar*$^-$, and *pir*A$^-$/*scar*$^-$ cells ($P < 0.01$). A representative experiment is shown; error bars show one standard deviation.

(B) Changes in F-actin during chemotaxis. A phalloidin binding assay was used to measure changes in F-actin levels in wild-type (AX3, diamonds), *pir*A$^-$ (squares), *pir*A$^-$/*scar*$^-$ (triangles), and *scar*$^-$ (crosses) cells, over time, in response to stimulation with 1 μM cAMP. F-actin values are given as a percentage of the F-actin content of unstimulated wild-type (AX3) cells.

(C) F-actin staining of *pir*A$^-$ mutants. Vegetative cells were stained with Alexa 546 phalloidin.

preexisting protrusions. Figure 4C shows a number of images taken 30 s apart from *pir*A$^-$ cells in an under-agar assay. Numerous new pseudopods can be seen, but essentially all of them appear to derive from the splitting of preexisting protrusions into two or three fragments. The newly split pseudopods then separate from one another by extending in different directions.

Taken together, the data in this work therefore suggest that PIR121, and by extension SCAR, is more directly involved in pseudopod modification and splitting than in de novo generation of new pseudopods.

Loss of SCAR Protein in *pir*A$^-$ Mutants

Given that the phenotype of *pir*A$^-$ cells is generally consistent with an inappropriate overactivation of SCAR, we were initially surprised to find very little intact SCAR protein in *pir*A$^-$ null cells. In fact, almost no full-length SCAR protein could be detected in *pir*A$^-$ cells by Western blotting, although a Northern blot shows no drop in *scar* mRNA levels (Figure 5). Haploid *pir*A null cells segregated from a heterozygous diploid strain, termed *pir*A$^-$*d*, also showed a loss of full-length SCAR (Figure 5).

It therefore appears that the loss of SCAR protein is due to posttranscriptional changes, not changes in *scar* gene expression. The simplest model proposes that in resting cells SCAR is protected within a complex of inhibitory proteins including PIR121. Disruption of the *pir*A gene would then lead to disassembly of the complex, leaving the SCAR protein both active and free to be downregulated by a process such as proteolysis.

Discussion

This work provides the first genetic connection between PIR121 and SCAR. We have provided in vivo support for previous work that suggested that PIR121 is a negative regulator that holds SCAR in an inactive conformation [16]. However, the phenotype we see is more complex than might be expected if loss of PIR121 disrupted connections between Rac and the Arp2/3 complex. First, there is a heavy emphasis on remodeling and splitting existing pseudopods, which has not been seen previously with mutants causing overactive Rac function. Secondly, the pathways connecting chemotactic signaling to actin polymerization seem not to be disrupted in *pir*A mutants. We also find that SCAR protein levels are sharply downregulated in the absence of PIR121, presumably by proteolysis.

Rac has been linked with SCAR function on a number of occasions [8, 16] and has been found or presumed to bind PIR121 by several groups [16, 17, 22]. This Rac connection demonstrated in mammalian cells is likely to be present in *Dictyostelium* because expression of overactive Rac proteins leads to cells with large numbers of pseudopods and high F-actin content [30, 33] in a phenotype similar to that presented here. Our data support the concept that PIR121 is a major link between SCAR and Rac and that binding of active Rac to PIR121 causes disassembly of the inhibitory complex and release of active SCAR, as previously suggested [16]. However, we find that the behavior of *pir*A$^-$ cells is different from that of mutants expressing overactive Rac

A

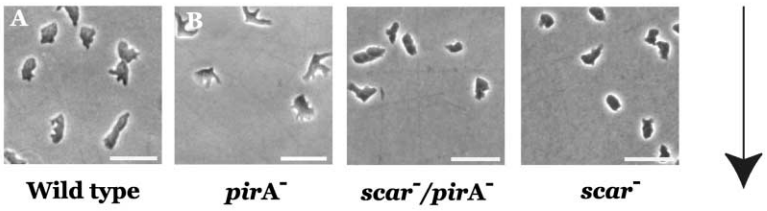

B

Analysis of speed and directionality of *Dictyostelium* mutants moving towards a folate gradient under agar

	Wild type	*pir*A⁻	*scar*⁻/*pir*A⁻	*scar*⁻
Chemotactic index	0.69	0.50	0.47	0.45
Cell speed (μm/min)	14.5 ± 2.0	9.9 ± 1.5	7.1±2.2	6.5 ± 1.2

C

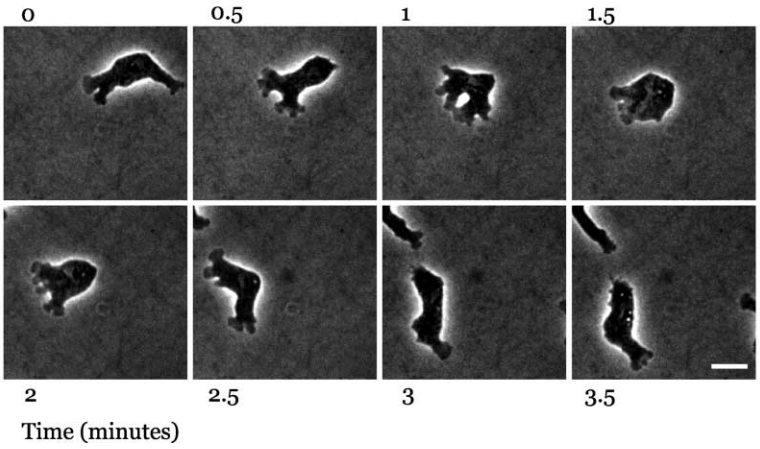

Figure 4. *pir*A⁻ and *scar*⁻ Cells Display Defects in Chemotaxis Under Agar

(A) Phase contrast images of chemotactic cells. *pir*A⁻ cells constantly split and remodel their pseudopods during under-agar chemotaxis, whereas *scar*⁻ null and *pir*A⁻/*scar*⁻ cells display decreased pseudopod splitting when compared to wild-type cells. The arrow represents general direction of cell movement toward the folate gradient. The scale bar represents 50 μm.

(B) Diminished speed and directional accuracy of mutant cells. Vegetative, axenically grown wild-type (AX3), *pir*A null, *scar* null, and *pir*A⁻/*scar*⁻ cells were filmed while moving under a layer of agar up a folate gradient and were analyzed to give rates of movement and chemotactic efficiency. Chemotactic indices of *pir*A⁻, *scar*⁻, and *pir*A⁻/*scar*⁻ are significantly different from those of the wild-type ($P < 0.05$), but not from each other. Cell speeds of wild-type and *pir*A⁻ cells are significantly different from each other and from *scar*⁻ and *pir*A⁻/*scar*⁻ cells ($P < 0.01$).

(C) The leading edges of *pir*A null cells constantly split. Phase contrast microscopy was used for filming cells moving under agar up a folate gradient. The frames were taken approximately 30 s apart. The scale bar is 10 μm.

proteins. In particular, *pir*A⁻ cells usually make new pseudopods at the leading edge by subdividing and remodeling previously existing actin structures, whereas Rac overexpressers usually initiate new pseudopods all over their surfaces in a nonpolar fashion (for review, see [33]). In *Dictyostelium*, *scar* null cells are capable of forming actin structures and extending pseudopods, albeit with less F-actin in their cells [9], whereas *pir*A null cells continually split existing lamellae and form numerous pseudopods. Our data therefore suggest that *Dictyostelium* SCAR has a major role in modification and splitting of pseudopods and other actin structures rather than in their initial generation. This role appears to be tightly controlled by PIR121 (and maybe other members of the inhibitory complex) in normal cells and is presumably controlled by signaling molecules, including Rac proteins.

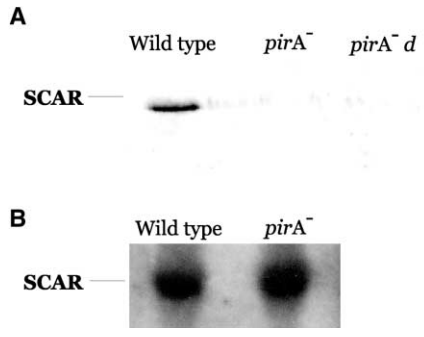

Figure 5. Loss of SCAR Protein in *pir*A⁻ Cells

(A) Western blot showing SCAR protein in vegetatively grown cells. Full-length SCAR protein is clearly visible in wild-type (AX3) cells but was almost undetectable in *pir*A null cells and in *pir*A⁻*d*, a haploid cell line segregated from a diploid *pir*A⁻ strain.

(B) Northern blot showing *scar* mRNA levels in vegetatively grown cells. No loss of *scar* mRNA is seen.

We have also suggested another mechanism for regulation of SCAR. We detected very little full-length SCAR protein in *pir*A null cells, but mRNA levels remain unchanged. This suggests that a posttranscriptional process, most likely proteolysis, is responsible for the lack of SCAR in *pir*A⁻ cells. In resting wild-type cells, SCAR is likely to be protected from downregulation by the inhibitory complex, but when the complex is disassembled in response to signals, SCAR would be left exposed to downregulation. In *pir*A null cells, there is no inhibitory complex, leaving SCAR active and therefore susceptible to downregulation at all times. It seems most likely that

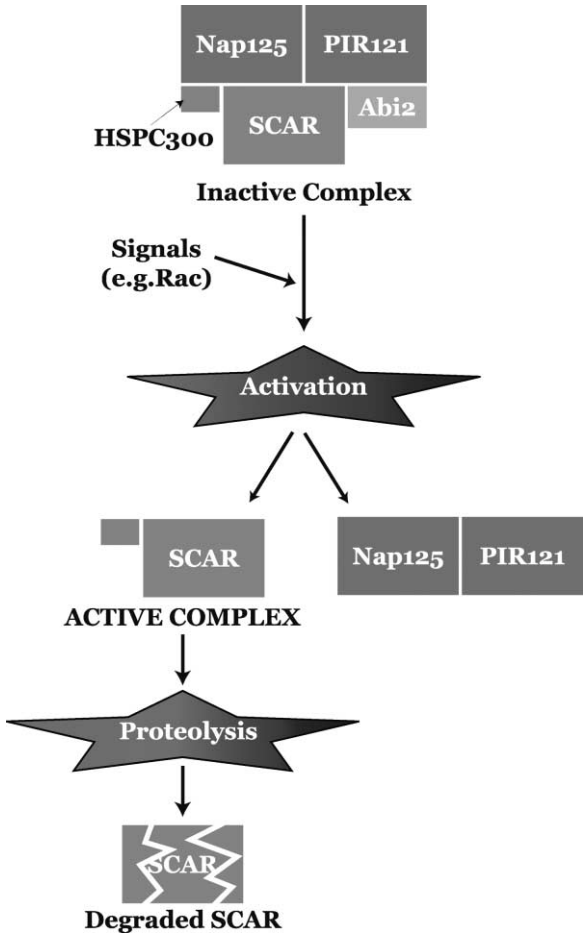

Figure 6. Model of the SCAR Regulation Cycle

SCAR normally exists in an inactive state as part of a complex of proteins, including Nap125, PIR121, HSPC300, and Abi2. External or internal signals promote disassembly of the complex into an active portion (SCAR and HSPC300) and an inactive portion (PIR121 and NAP125), leaving active SCAR at the leading edge where it promotes actin polymerization through the Arp2/3 complex. Free SCAR, unlike SCAR in the active complex, is susceptible to rapid breakdown, presumably by proteolysis.

rapid proteolysis of active SCAR limits its activity and that this is what turns off activation of actin nucleation. This process could act in concert with reassociation of the inhibitory complex, or instead of it. We would therefore like to expand on the recent model by Eden et al and suggest a model of SCAR regulation involving breakdown (Figure 6). Suggesting a very high rate of turnover of SCAR, this model proposes that SCAR is continually made and broken down after performing its function at the leading edge.

Future work will focus on the nature of this proteolysis and whether it is the principal method of halting the SCAR signal, as well as the biological roles of conserved SCAR-connected proteins, such as Nap125, Abi2, and HSPC300.

Conclusions

We have provided evidence that PIR121 exists in a complex with SCAR and functions to inhibit SCAR in vivo in the absence of signaling. In the absence of SCAR, loss of PIR121 has no obvious effect. We also show that SCAR has important roles in pseudopod modification and splitting in *Dictyostelium* and that disruption of normal SCAR regulation leads to severe defects in this area. We suggest that once active SCAR is released from its inhibitory complex, it is rapidly removed and that this mechanism is important to the normal regulation of actin dynamics.

Experimental Procedures

Cell Culture and Development

Dictyostelium cells were grown axenically in HL-5 medium at 22°C either in Petri dishes or in shaken flasks. For experiments requiring bacterially grown cells, *Dictyostelium* were plated onto lawns of *Klebsiella aerogenes* and harvested after 48 hr by repeated washing in KK_2 buffer. For experiments requiring developed cells, *Dictyostelium* were harvested from *Klebsiella* lawns, starved for 1 hr by being shaken in KK_2 buffer, then treated with 0.1 μM cAMP every 6 min for 4 hr while being slowly shaken at a density of 2×10^7/ml.

Generation of Gene Disruptants

The *Dictyostelium discoideum* homologs of PIR121 and the other members of the complex were identified by BLAST searches against the libraries of the Tsukuba *Dictyostelium* cDNA project and the *Dictyostelium* genome project in Köln. A 1.4 kbp section of the *pir*A gene was amplified from genomic DNA by PCR with the primers GAATCTGCAGTCGAAGCTTGCGATTTAACA (upstream) and GAA TGCGGCCGCAGGTGGTGAAAGGATCA (downstream). The resulting segment was then cloned into pBluescript, and subsequently a blasticidin resistance cassette was cloned into a BamHI site in the gene. This construct was electroporated into *Dictyostelium* AX3 cells, and subsequent blasticidin resistant colonies were screened for gene disruption via PCR and Southern blotting.

To make double *pir*A/*scar* mutants, a new *scar*$^-$ mutant was generated by uracil selection. The pScar1 cDNA (a kind gift of Dr. Karl Saxe) was trimmed with SacI and SmaI to remove the XbaI site from the polylinker, then cut with XbaI and ClaI. An XbaI-ClaI fragment containing the full-length *pyr*56 gene from pRHI62 was inserted to give a construct containing 430 bp of 5′ and 1100 bp of 3′ *scar* sequence interrupted by *pyr*56. This was transfected into *pyr*56$^-$ JH8 cells, which were then selected in minimal FM medium. Clones were screened by Western blot, with one-eighth proving to be clean knockouts. The double *pir*A/*scar* mutant was constructed from these *scar*$^-$ cells as the parental strain, with the *pir*A gene disrupted with the same construct used for generating the original *pir*A$^-$ mutant.

Actin Polymerization Assays

To determine the proportion of F-actin in resting cells, we used a previously described method to isolate triton-insoluble cytoskeletal proteins [34, 35]. Test samples of cytoskeleton and also varying amounts of total cell lysate in which the soluble G-actin had not been removed were run on a large SDS-PAGE gel. Gels were then stained with Coomassie blue dye, scanned into a computer, and quantitated with NIH Image.

To determine changes in F-actin over time in response to 1 μM cAMP stimulation, we used a phalloidin-based assay as previously described [31, 36] on developed *Dictyostelium* cells.

Under Agar Chemotaxis Assays

We used the previously described method for imaging *Dictyostelium* cells moving toward a folate stimulus under a thin layer of agarose [32]. In brief, three troughs (2 mm wide) were cut into thin layers of 1% SM agar in Petri dishes. The center trough was then filled with 100 μl of 0.1 mM folic acid, and 100 μl of log phase, axenically growing cells at a density of around 1×10^6/ml were added to troughs either side of the folic acid. We then imaged the cells as they moved under the agar toward the folate stimulus by using phase contrast microscopy over the next 6–8 hr.

Cell Speed and Chemotaxis

To measure cell movement, we imaged bacterially grown cells by using DIC microscopy, and we calculated cell speeds by using an NIH image macro to calculate the mean displacement of cell centroids and sampling frames every 20 s. To measure chemotaxis, we imaged vegetative cells moving under agar toward a folate gradient by using phase-contrast microscopy. We measured chemotactic indices by calculating the cosines of the angle of difference between successive frames at 30 s intervals.

Antibody Production

For production of the SCAR fragment, a construct containing the N-terminal sequence corresponding to the SCAR homology domain was cloned into the expression vector pMW172. Inclusion bodies were induced, purified, and prepared as described previously [37]. Rabbit polyclonal antibodies were produced from PAGE gel-purified protein by Eurogentec. The antiserum was affinity purified as described in [37].

Acknowledgments

We are very grateful to Dr. David Knecht for his help in setting up the under-agar chemotaxis system and to Dr. Karl Saxe for the pScar1 clone. We thank Dr. Laura Machesky for constructive comments on the manuscript and Drs. Knecht, Saxe, and Machesky for constant discussion of the results. We thank the Japanese cDNA project for clones. R.H.I. is supported by an MRC Senior Fellowship, and S.L.B. is supported by a Biotechnology and Biological Sciences Research Council postgraduate studentship.

Received: April 4, 2003
Revised: July 24, 2003
Accepted: July 24, 2003
Published: September 2, 2003

References

1. Machesky, L.M., Atkinson, S.J., Ampe, C., Vandekerckhove, J., and Pollard, T.D. (1994). Purification of a cortical complex containing two unconventional actins from Acanthamoeba by affinity-chromatography on profilin-agarose. J. Cell Biol. *127*, 107–115.
2. Mullins, R.D., Heuser, J.A., and Pollard, T.D. (1998). The interaction of Arp2/3 complex with actin, nucleation, high affinity pointed end capping, and formation of branching networks of filaments. Proc. Natl. Acad. Sci. USA *95*, 6181–6186.
3. Machesky, L.M., and Insall, R.H. (1998). Scar1 and the related Wiskott-Aldrich syndrome protein, WASP, regulate the actin cytoskeleton through the Arp2/3 complex. Curr. Biol. *8*, 1347–1356.
4. Zalevsky, J., Lempert, L., Kranitz, H., and Mullins, R.D. (2001). Different WASP family proteins stimulate different Arp2/3 complex-dependent actin-nucleating activities. Curr. Biol. *11*, 1903–1913.
5. Derry, J.M., Ochs, H.D., and Francke, U. (1994). Isolation of a novel gene mutated in Wiskott-Aldrich syndrome. Cell *78*, 635–644.
6. Miki, H., Sasaki, T., Takai, Y., and Takenawa, T. (1998a). Induction of filopodium formation by a WASP-related actin depolymerising protein N-WASP. Nature *391*, 93–96.
7. Suetsugu, S., Miki, H., and Takenawa, T. (1999). Identification of two human WAVE/SCAR homologues as general actin regulatory molecules which associate with the Arp2/3 complex. Biochem. Biophys. Res. Commun. *260*, 296–302.
8. Miki, H., Suetsugu, S., and Takenawa, T. (1998b). WAVE, a novel WASP-family protein involved in actin reorganisation induced by Rac. EMBO J. *17*, 6932–6941.
9. Bear, J.E., Rawls, J.F., and Saxe, C.L. (1998). SCAR, a WASP-related protein, isolated as a suppressor of receptor defects in late *Dictyostelium* development. J. Cell Biol. *142*, 1325–1335.
10. Machesky, L.M., Mullins, R.D., Higgs, H.N., Kaiser, D.A., Blanchoin, L., May, R.C., Hall, M.E., and Pollard, T.D. (1999). Scar, a WASP-related protein activates nucleation of actin filaments by the Arp2/3 complex. Proc. Natl. Acad. Sci. USA *96*, 3739–3744.
11. Zallen, J.A., Cohen, Y., Hudson, A.M., Cooley, L., Wieschaus, E., and Schejter, E.D. (2002). SCAR is a primary regulator of Arp2/3-dependent morphological events in Drosophila. J. Cell Biol. *156*, 689–701.
12. Symons, M., Derry, J.M.J., Karlak, B., Jiang, S., Lemahieu, V., McCormick, F., Francke, U., and Abo, A. (1996). Wiskott-Aldrich syndrome protein, a novel effector for the GTPase CDC42Hs, is implicated in actin polymerization. Cell *84*, 723–734.
13. Higgs, H.D., and Pollard, T.P. (2000). Wiskott-Aldrich Syndrome protein (WASP) activation of Arp2/3 complex, effects of phosphatidylinositol-4,5-bisphosphate and Cdc42. J. Cell Biol. *150*, 1311–1320.
14. Rohatgi, R., Ho, H., and Kirschner, M.W. (2000). Mechanism of N-WASP activation by CDC42 and Phosphatidylinositol 4,5-bisphosphate. J. Cell Biol. *150*, 1299–1309.
15. Hahne, P., Sechi, A., Benesch, S., and Small, V. (2001). Scar/WAVE is localised at the tips of protruding lamellipodia in living cells. FEBS Lett. *492*, 215–220.
16. Eden, S., Rohatgi, R., Podtelejnikov, A.V., Mann, M., and Kirschner, M.W. (2002). Mechanism of regulation of WAVE1-induced actin nucleation by Rac1 and Nck. Nature *418*, 790–793.
17. Kitamura, T., Kitamura, Y., Yonezawa, K., Totty, N.F., Gout, I., Hara, K., Waterfield, M.D., Sakaue, M., Ogawa, W., and Kasuga, M. (1996). Molecular cloning of $p125^{Nap1}$, a protein that associates with an SH3 domain of Nck. Biochem. Biophys. Res. Commun. *219*, 509–514.
18. Suzuki, T., Nishiyama, K., Yamamoto, A., Inazawa, J., Iwaki, T., Yamada, T., Kanazawa, I., and Yoshiyuki, S. (1999). Molecular cloning of a novel apoptosis-related gene, human Nap1 (NCKAP1), and its possible relation to Alzheimer Disease. Genomics *63*, 246–254.
19. Yamamoto, A., and Behl, C. (2001). Human Nck-associated protein1 and its binding protein affect the metabolism of beta-amyloid precursor protein with Swedish mutation. Neurosci. Lett. *316*, 50–54.
20. Kitamura, Y., Kitamura, T., Sakaue, H., Maeda, T., Ueno, H., Nishio, S., Ohno, S., Osada, S., Sakaue, S., Ogawa, W., et al. (1997). Interaction of Nck-associated protein 1 with activated GTP-binding protein Rac. Biochem. J. *322*, 873–878.
21. Saller, E., Tom, E., Brunori, M., Lotter, M., Estreicher, A., Mack, D.H., and Iggo, R. (1999). Increased apoptosis induction by 121F mutant p53. EMBO J. *18*, 4424–4437.
22. Kobayashi, K., Kuroda, S., Fukata, M., Nakamura, T., Nagase, T., Nomura, N., Matsuura, Y., Yoshida-Kubomura, N., Iwamatsu, A., and Kaibuchi, K. (1998). p140SRA-1 (specifically Rac1-associated protein) is a novel specific target for Rac small GTPase. J. Biol. Chem. *273*, 291–295.
23. Daiz, Z., and Pendergast, A.M. (1995). Abi-2, a novel SH3-containing protein interacts with the c-Abl tyrosine kinase and modulates c-Abl transforming activity. Genes Dev. *9*, 2569–2582.
24. Stradal, T., Courtney, K.D., Rottner, K., Hahne, P., Small, J.V., and Pendergast, A.M. (2001). The Abl interactor proteins localize to sites of actin polymerisation at the tips of lamellipodia and filopodia. Curr. Biol. *11*, 891–895.
25. Soto, M.C., Qadoto, H., Kasuya, K., Inoue, M., Tsuboi, D., Mello, C.C., and Kaibuchi, K. (2002). The GEX-2 and GEX-3 proteins are required for tissue morphogenesis and cell migrations in C. elegans. Genes Dev. *16*, 620–632.
26. Tuxworth, R.I., Cheetham, J.L., Machesky, L.M., Spiegelmann, G.B., Weeks, G., and Insall, R.H. (1997). *Dictyostelium* RasG is required for normal motility and cytokinesis, but not growth. J. Cell Biol. *138*, 605–614.
27. Chung, C.Y., Potikyan, G., and Firtel, R.A. (2001). Control of cell polarity and chemotaxis by Akt/PKB and PI3 kinase through the regulation of PAKa. Mol. Cell *7*, 937–947.
28. Svitkina, T.M., and Borisy, G.G. (1999). Progress in protrusion: the tell-tale scar. Trends Biochem. Sci. *24*, 432–436.
29. Haugwitz, M., Noegel, A.A., Karakesisoglou, J., and Schleicher, M. (1994). *Dictyostelium* amoebae that lack G-actin sequestering profilins show defects in F-actin content, cytokinesis, and development. Cell *79*, 303–314.
30. Chung, C.Y., Lee, S., Briscoe, C., Ellsworth, C., and Firtel, R.A.

(2000). Role of Rac in controlling the actin cytoskeleton and chemotaxis in motile cells. Proc. Natl. Acad. Sci. USA *97*, 5225–5230.

31. Hall, A.L., Schlein, A., and Condeelis, J. (1988). Relationship of pseudopod extension to chemotactic hormone-induced actin polymerization in amoeboid cells. J. Cell. Biochem. *37*, 285–299.
32. Laevsky, G., and Knecht, D.A. (2001). Under-agarose folate chemotaxis of *Dictyostelium discoideum* amoebae in permissive and mechanically inhibited conditions. Biotechniques *31*, 1140–1149.
33. Wilkins, A., and Insall, R.H. (2001). Small GTPases in *Dictyostelium*: lessons from a social amoeba. Trends Genet. *17*, 41–48.
34. Brown, S., Levinson, W., and Spudich, J.A. (1976). Cytoskeletal elements of chick embryo fibroblasts revealed by detergent extraction. J. Supramol. Struct. *5*, 119–130.
35. McRobbie, S.J., and Newell, P.C. (1983). Changes in actin associated with the cytoskeleton following chemotactic stimulation of *Dictyostelium discoideum*. Biochem. Biophys. Res. Commun. *115*, 351–359.
36. Peracino, B., Borleis, J., Jin, T., Westphal, M., Schwartz, J.M., Wu, L., Bracco, E., Gerisch, G., Devreotes, P., and Bozzaro, S. (1998). G protein beta subunit-null mutants are impaired in phagocytosis and chemotaxis due to inappropriate regulation of the actin cytoskeleton. J. Cell Biol. *141*, 1529–1537.
37. Insall, R., Müller-Taubenberger, A., Machesky, L., Köhler, J., Simmeth, E., Atkinson, S.J., Weber, I., and Gerisch, G. (2001). Dynamics of the *Dictyostelium* Arp2/3 Complex in Endocytosis, Cytokinesis, and Chemotaxis. Cell Motil. Cytoskeleton *50*, 115–128.